Supporting Material: Bifurcation of velocity distributions in cooperative transport of filaments by fast and slow motors

Xin Li[1], Reinhard Lipowsky[1], Jan Kierfeld[1,2]

[1]Max Planck Institute of Colloids and Interfaces, Science Park Golm, 14424 Potsdam, Germany
[2]Physics Department, TU Dortmund University, 44221 Dortmund, Germany

December 10, 2012

Section 1 of the Supporting Material contains the master equation used in the theoretical analysis as well as the derivation of binding and unbinding rates in the master equation. We also discuss frictional forces. In section 2, we give analytical estimates for the boundaries η_l and η_u of the bistable regime in the mean field motility diagrams, Section 3 contains additional motility diagrams in the $(\hat{F}, \frac{N_f}{N})$ and $(\hat{v}, \frac{N_f}{N})$ parameter planes. In section 4, we discuss the influence of the total number of available motors N on our results.

1 Master equation approach

We assume fixed numbers N_f of fast and N_s of slow motors available to attach to the microtubule. The numbers of n_f fast and n_s slow motors that actually bind and transport the microtubule vary stochastically in $0 \leq n_f \leq N_f$ and $0 \leq n_s \leq N_s$ because of stochastic binding and unbinding of motors, see Fig. 3 A in the main text. The state of the filament can then be uniquely described by the pair (n_f,n_s) of motor numbers. Let $p(n_f, n_s, t)$ denote the probability to find the filament with n_f fast and with n_s slow motors attached at time t, then the stochastic properties of the system

are described by the master equation

$$\begin{aligned}\frac{\partial}{\partial t}p(n_f,n_s,t) &= \epsilon_f(n_f+1,n_s)p(n_f+1,n_s,t)+\epsilon_s(n_f,n_s+1)p(n_f,n_s+1,t)\\ &+\pi_f(n_f-1,n_s)p(n_f-1,n_s,t)+\pi_s(n_f,n_s-1)p(n_f,n_s-1,t)\\ &-[\pi_f(n_f,n_s)+\pi_s(n_f,n_s)+\epsilon_f(n_f,n_s)+\epsilon_s(n_f,n_s)]p(n_f,n_s,t) \quad \text{(S1)}\end{aligned}$$

where π_f and ϵ_f are the rates for binding and unbinding of fast motors, as well as π_s and ϵ_s are the rates for binding and unbinding of slow motors. All four rates depend on the state (n_f,n_s) of the system.

We take the binding rate of a single motor to be independent of load force because unbound motors can always bind to filaments from their relaxed state, which means $\pi(F)=\pi_0$ is independen of force and equals the zero load force binding rate π_0 (1, 2). The single motor unbinding rate depends on its load force F and is given by (3, 4)

$$\epsilon(F)=\epsilon_0\exp(|F|/F_d), \quad \text{(S2)}$$

where ϵ_0 is the unbinding rate at zero load force, and F_d defines the detachment force. The detachment force F_d can be different for forces in the forward and backward direction of motor motion.

For the systems studied in this article, fast motors will always experience resisting forces because they move faster, while slow motors will be pulled forward and experience assisting forces. We use the convention that resisting forces F have positive sign, and assisting forces have negative sign.

For a fast motor under a resisting force $F\geq 0$, we assume an approximately linear force-velocity relation (4–7)

$$\mathcal{V}_f(F)=v_f(1-F/F_{sf}) \quad \text{for} \quad 0\leq F<F_{sf}, \quad \text{(S3)}$$

where v_f is the velocity of the unloaded fast motor. If the motor is pulled backwards by resisting forces exceeding a stall force F_{sf}, i.e., for $F\geq F_{sf}$, we assume that it stalls resulting in $\mathcal{V}(F)=0$.

For a slow motor under an assisting force $F\leq 0$, the motor velocity increases as observed in experiments (7, 8), and we assume a linear relation

$$\mathcal{V}_s(F)=v_s(1-F/F_{ss}) \quad \text{for} \quad F\leq 0<F_{ss}, \quad \text{(S4)}$$

where v_s is the velocity of an unloaded slow motor and F_{ss} is a characterstic force, which gives the intersection point of the force-velocity curve with the force-axis as

indicated in Fig. 3 B in the main text. In principle, the force F_{ss} characterizing the force-velocity relation in the regime of assisting forces $F \leq 0$ can be different from the stall force of slow motors. We assume $F_s \equiv F_{ss} = F_{sf}$ for simplicity.

The effective binding and unbinding rates in a state (n_f,n_s) depend on the load force on each motor and can be calculated from the conditions of (i) force balance and equal force sharing and (ii) equal velocities of all motors in a stationary state with respect to motor motion. This assumes that motor stepping happens at a time scale, which is small compared to the time scale for binding and unbinding of motors such that we can use conditions (i) and (ii) with fixed motor numbers n_s and n_f.

Because of the different stepping velocities, an assisting load force $F_- < 0$ is acting on each slow motor, whereas a resisting load force $F_+ > 0$ is acting on each fast motor. We assume that the total load is equally shared between all n_f attached fast and all n_s attached slow motors. Therefore, the condition (i) of force balance on the microtubule leads to

$$n_f F_+ = -n_s F_- \equiv F(n_f, n_s), \tag{S5}$$

where $F(n_f, n_s) > 0$ is the absolute value of the total force acting on each motor group. In eq. (S5) we assumed that we can neglect frictional forces on the moving filament in the force balance and that the filament is very stiff, such that we need not consider elastic forces explicitly. If we include the friction force Γv_m for a microtubule with velocity v_m and friction coefficient Γ (with $\Gamma = 2\pi\eta L/\ln(L/D)$ for motion along the microtubule axis, where η is the viscosity of the surrounding liquid, L the microtubule length, and D the microtubule diameter) into the force balance, we obtain

$$n_f F_+ + n_s F_- = \Gamma v_m. \tag{S6}$$

For a typical microtubule velocity $v_m = 1\,\mu$m/s, microtubule length $L = 5\,\mu$m and diameter $D = 25\,$nm, and the viscosity of water $\eta = 10^{-3}\,Ns/m^2$, the friction force is only $\sim 6 \times 10^{-3}\,$pN and can be neglected.

Given the unbinding rate of a single motor as in equation (S2), the effective unbinding rates ϵ_f and ϵ_s of n_f fast and n_s slow motors from the microtubule in the state (n_f, n_s) are

$$\epsilon_f(n_f, n_s) = n_f \epsilon_{0f} \exp[F(n_f, n_s)/(n_f F_{df})] \tag{S7}$$

$$\epsilon_s(n_f, n_s) = n_s \epsilon_{0s} \exp[F(n_f, n_s)/(n_s F_{ds})]. \tag{S8}$$

The parameters ϵ_{0f} and ϵ_{0s} denote the unbinding rates of a single fast and slow motor at zero load force, and F_{df} and F_{ds} denote the detachment forces for fast and slow

motors, respectively. Similarly, the effective binding rates π_f and π_s of fast and slow motors in state (n_f, n_s) are

$$\pi_f(n_f, n_s) = (N_f - n_f)\pi_{0f} \tag{S9}$$
$$\pi_s(n_f, n_s) = (N_s - n_s)\pi_{0s}, \tag{S10}$$

where $N_f - n_f$ and $N_s - n_s$ are the numbers of unbound fast and slow motors which are available to bind to the microtubule, respectively. The parameters π_{0f} and π_{0s} denote the corresponding binding rates of fast and slow motors.

The condition (ii) of equal velocities of all motors leads to

$$\mathcal{V}_f(F_+) = \mathcal{V}_s(F_-) = v_m(n_f, n_s), \tag{S11}$$

where $\mathcal{V}_f$ and $\mathcal{V}_s$ are the velocities of individual fast and slow motors as given by the force-velocity relations (S3) and (S4), respectively, and v_m is the velocity of the microtubule.

Combining the condition (S11) of equal velocities and the force balance relation (S5), we can eliminate F_+ and F_- and obtain the microtubule velocity

$$v_m(n_f, n_s) = \frac{v_s v_f}{(1 - \frac{n_f}{n})v_f + \frac{n_f}{n} v_s}, \tag{S12}$$

where v_f and v_s are the velocities of fast and slow motors at zero load force, respectively, and $n \equiv n_f + n_s$ is the total number of bound motors. We also obtain the total force $F(n_f, n_s)$ acting on each motor group,

$$F(n_f, n_s) = \frac{1 - \frac{v_s}{v_f}}{1 + \frac{n_f}{n_s}\frac{v_s}{v_f}} n_f F_s. \tag{S13}$$

Using this expression in eqs. (S7) and (S8), we can calculate the effective unbinding rates in a state (n_f, n_s) characterized by the numbers of bound fast and slow motors. This determines the effective rates in the master equation (S1).

In the presence of friction, we find from the condition (S11) of equal velocities and the modified force balance relation (S6) the generalized relations

$$v_m(n_f, n_s) = \frac{v_s v_f}{(1 - \frac{n_f}{n})v_f + \frac{n_f}{n} v_s + \frac{\Gamma v_f v_s}{n F_s}} \ , \tag{S14}$$

and

$$n_f F_+ = \frac{1 - \frac{v_s}{v_f} + \frac{v_s}{v_f}\frac{\Gamma v_m}{n_s F_s}}{1 + \frac{n_f}{n_s}\frac{v_s}{v_f}} n_f F_s \tag{S15}$$

$$-n_s F_- = \frac{1 - \frac{v_s}{v_f} - \frac{\Gamma v_m}{n_f F_s}}{1 + \frac{n_f}{n_s}\frac{v_s}{v_f}} n_f F_s \tag{S16}$$

which reduce to eqs. (S12) and (S13) for $\Gamma = 0$.

2 Analytical estimates for stability boundaries in motility diagrams

The mean field equation for the parameter

$$f_{\mathrm{MF}}(\hat{n}) \equiv \frac{\hat{v}}{\hat{N}} \frac{\exp\left[\frac{\hat{F}(1-\hat{v})}{\eta\hat{v}}\frac{\hat{n}}{1+\hat{n}}\right] + \hat{\pi}}{\exp\left[\frac{\hat{F}(1-\hat{v})}{1+\hat{n}}\right] + \hat{\pi}} = \hat{n}, \tag{S17}$$

for the parameter

$$\hat{n} \equiv \frac{\langle n_f \rangle}{\langle n_s \rangle}\frac{v_s}{v_f}, \tag{S18}$$

see eqs. (23) and (24) in the main text, can have one, two, or three different solutions. The parameter regime of bistable transport is characterized by the existence of three solutions in mean field theory. At the boundaries of this regime, there are saddle node bifurcations, and eq. (S17) has two solutions, see Fig. 4 in the main text. These boundaries are determined by the additional bifurcation condition $f'_{\mathrm{MF}}(\hat{n}) = 1$. By solving $f_{\mathrm{MF}}(\hat{n}) = \hat{n}$ and $f'_{\mathrm{MF}}(\hat{n}) = 1$ simultaneously, we obtain the critical values η_l and η_u at the lower and upper boundary, respectively, as a function of the fraction of fast motors N_f/N. Outside the bistable regime for $\eta < \eta_l$ or $\eta > \eta_u$, the mean field equation (S17) has only a single solution. Apart from calculating η_l and η_u numerically from the conditions $f_{\mathrm{MF}}(\hat{n}) = \hat{n}$ and $f'_{\mathrm{MF}}(\hat{n}) = 1$, as we did for the red data points in the motility diagrams in Fig. 5 in the main text, analytical estimates can be given working in the limits of small and large $\hat{n}$.

In the limit of small $\hat{n} = n_f/n_s \ll 1$, i.e., small ratios of fast to slow attached motors, we obtain the lower branch η_l of critical values, as can be seen from the

bifurcation diagram in Fig. 4 in the main text. Expanding the arguments of both exponentials in the function $f_{\rm MF}(\hat{n})$ in the mean-field equation (S17) for $\hat{n} \ll 1$ gives

$$f_{\rm MF}(\hat{n}) \approx \frac{\hat{v}}{\hat{N}} \frac{\exp\left[\frac{\hat{F}(1-\hat{v})}{\eta\hat{v}}\hat{n}\right] + \hat{\pi}}{\exp\left[\hat{F}(1-\hat{v})\right] + \hat{\pi}} = \hat{n}. \tag{S19}$$

Using this approximation, the equations $f_{\rm MF}(\hat{n}) = \hat{n}$ and $f'_{\rm MF}(\hat{n}) = 1$ can be solved analytically to obtain η_l. We find a simple $1/\hat{N}$-dependence for the lower branch of critical values,

$$\eta_l = \frac{1}{\hat{N}} \frac{W(\hat{\pi})\hat{F}(1-\hat{v})}{\exp[\hat{F}(1-\hat{v})] + \pi}, \tag{S20}$$

see eq. (5) in the main text. In eq. (S20), the function $W(x)$ is the positive branch of the Lambert W-function, which is the solution of $x = We^W$ for $W \geq -1$. For $\hat{\pi} = 5$, we have $W(\hat{\pi}) \simeq 6.14$.

For the parameter values for the three gliding assay systems given in Table 1 in the main text, we then find $\eta_l \simeq 1.00/\hat{N}$ (solid blue curve in Fig. 5 A in the main text) for wild-type and mutant kinesin-1, $\eta_l \simeq 0.61/\hat{N}$ (solid blue curve in Fig. 5 B in the main text) for OSM-3 and kinesin-II motors, and $\eta_l \simeq 0.74/\hat{N}$ (solid blue curve in Fig. 5 C in the main text) for Xklp1 and Xkid motors. All estimates show good agreement with the numerical calculation, in particular for small fraction of fast motors N_f/N.

In the limit of large $\hat{n} = n_f/n_s \gg 1$, i.e., a large ratio of fast to slow attached motors, we obtain the upper branch η_u of critical values, as can be seen from the bifurcation diagram in Fig. 4 in the main text. We can obtain an approximate closed expression for η_u by expanding the arguments of the exponentials in the mean-field equation (S17) in $1/\hat{n} \ll 1$ and by neglecting $\hat{\pi}$ in the nominator, which is justified for small $\hat{v}$,

$$f_{\rm MF}(\hat{n}) \approx \frac{\hat{v}}{\hat{N}} \frac{\exp\left[\frac{\hat{F}(1-\hat{v})}{\eta\hat{v}}(1-1/\hat{n})\right]}{1+\hat{\pi}} = \hat{n}. \tag{S21}$$

With these approximations, $f_{\rm MF}(\hat{n}) = \hat{n}$ and $f'_{\rm MF}(\hat{n}) = 1$ can be solved analytically, and we find

$$\eta_u = \frac{\hat{F}(1-\hat{v})}{\hat{v}} \frac{1}{-W_-\left[-\frac{\hat{v}}{\hat{N}(1+\hat{\pi})e}\right]}, \tag{S22}$$

where $W_-(x)$ is the negative branch of the Lambert W-function, which is the solution of $x = We^W$ for $W \leq -1$. The asymptotics $W_-(-x) \approx \ln(x)$ for $0 < x \ll 1$ gives a

logarithmic dependence

$$\eta_u \propto 1/\ln \hat{N} \tag{S23}$$

for $\hat{v}/\hat{N} \ll 1$, see eq. (6) in the main text.

Alternatively, we observe that $\hat{n}$ changes very slowly as a function of N_f/N along the upper branch η_u of critical values. Therefore, we use a constant approximation $\hat{n} \approx \hat{n}_0$ along the upper branch, which also leads to a logarithmic dependence of the form (S23),

$$\eta_u = \frac{\hat{F}(1-\hat{v})}{\hat{v}} \frac{\hat{n}_0}{1+\hat{n}_0} \frac{1}{\ln\left[\hat{N}\frac{\hat{n}_0}{\hat{v}}\left(\exp\left[\frac{\hat{F}(1-\hat{v})}{1+\hat{n}_0}\right]+\hat{\pi}\right)-\hat{\pi}\right]} \propto 1/\ln \hat{N}. \tag{S24}$$

We find that values $\hat{n}_0 = 5.0$ give good approximations of the upper critical branch for all three gliding assays, as shown by green solid lines in Fig. 5.

3 Motility diagrams in the $(\hat{F}, \frac{N_f}{N})$ and $(\hat{v}, \frac{N_f}{N})$ parameter planes

From the mean field equation (S17) we identify the ratio of detachment forces $\eta = F_{ds}/F_{df}$, the velocity mismatch between slow and fast motors $\hat{v} = v_s/v_f$, and the ratio of stall and detachment force $\hat{F} = F_s/F_{df}$ as most relevant microscopic motor parameters, as well as the fraction $N_f/N = 1/(1+\hat{N})$ of available fast motors as most relevant experimental control parameter.

In the main text, we discuss in detail the motility diagrams in the $(\frac{N_f}{N}, \eta)$ parameter plane for three gliding assay experiments. In this section, we discuss additional motility diagrams in the $(\hat{F}, \frac{N_f}{N})$ and $(\hat{v}, \frac{N_f}{N})$ parameter planes in Figs. S1 and S2. For the three different gliding assay experiments we used motor parameters from Table 1 in the main text.

Also as a function of the parameters $\hat{F}$ and $\hat{v}$, the mean-field equation (S17) can have one, two, or three different solutions. We find an analogous bifurcation behavior as in the $(\frac{N_f}{N}, \eta)$ parameter plane: there exists a bistable motility regime in the parameter plane, where we find two stable and one unstable solution, whereas we have only a single solution branch outside this region. At the critical parameter values at the boundaries of the bistable regime, the single solution bifurcates in a saddle node bifurcation. Bistability corresponds to a bimodal velocity distribution in the master equation approach and to bistable transport, whereas a single solution corresponds to a unimodal velocity distribution, i.e., fast or slow transport.

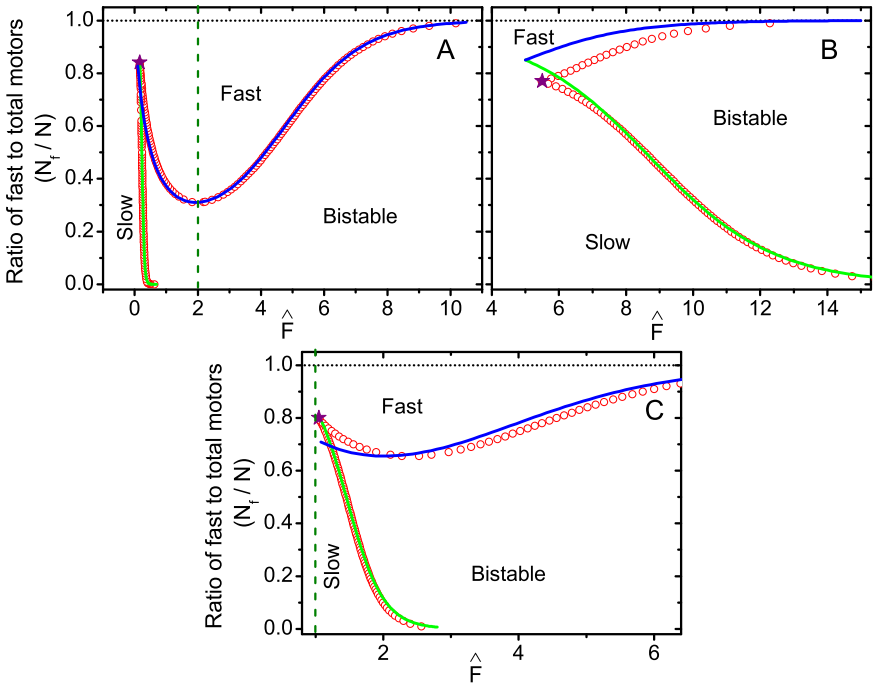

Figure S1: Motility diagrams for microtubules transported by (A) wild and mutant type of kinesin-1 motors, (B) OSM-3 and kinesin-II motors, (C) Xklp1 and Xkid motors as a function of the parameters $\hat{F}$ and N_f/N. The regime on the lower right enclosed by the open circles is the regime of bistable transport, while we find fast or slow transport with a unimodal velocity distribution outside this region. The open circles are numerical results, the solid blue and green curves are obtained from the analytical approximations (S20) and (S24), respectively. The stars indicate critical points. The dashed green lines represent the parameters explored experimentally in (A) Ref. (9) and (C) Ref. (10).

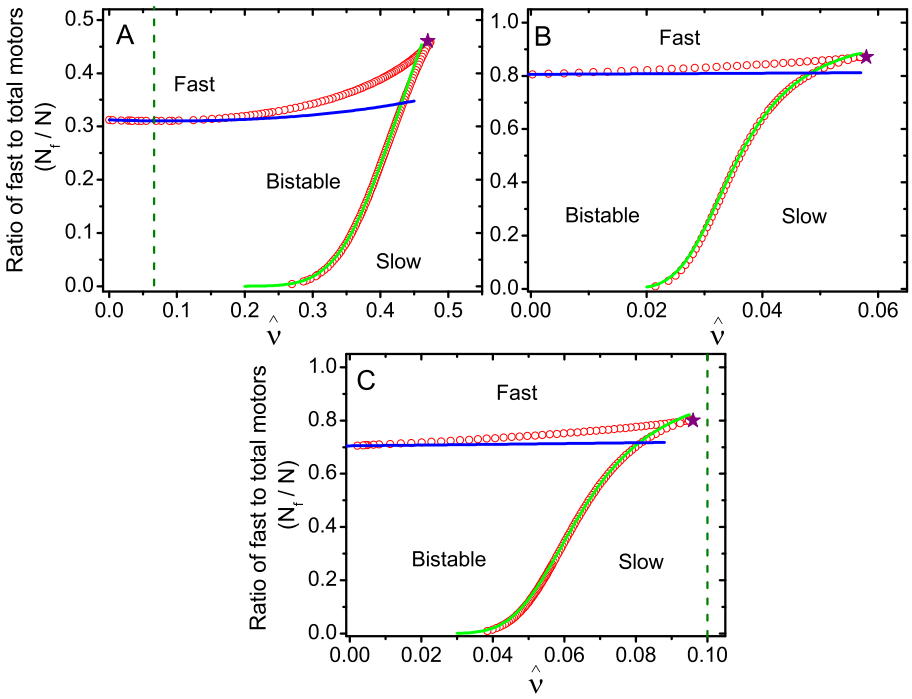

Figure S2: Motility diagrams for microtubules transported by (A) wild and mutant type of kinesin 1 motors, (B) OSM-3 and kinesin-II motor, (C) Xklp1 and Xkid motors as a function of the parameters $\hat{v}$ and N_f/N. In the regime on the lower left enclosed by the open circles we find bistable transport. Outside this region we find fast or slow transport with a unimodal velocity distribution. The open circles are numerical results, the solid blue and green curves are obtained from the analytical approximations (S20) and (S24), respectively. The stars indicate critical points. The dashed green lines represent the parameters explored experimentally in (A) Ref. (9) and (C) Ref. (10).

The critical values at the boundaries of the bistable parameter regions can be determined by simultaneous solution of the mean-field equation $f_{\mathrm{MF}}(\hat{n}) = \hat{n}$ and the condition $f'_{\mathrm{MF}}(\hat{n}) = 1$ resulting in the open red circles in Figs. S1 and S2. The boundaries of the bistable parameter regions consist of two branches, which terminate in a critical point, where the additional condition $f''_{\mathrm{MF}}(\hat{n}) = 0$ holds (marked by a star in Figs. S1 and S2).

We can obtain analytical estimates for the two boundary lines of critical values using a small $\hat{n}$ approximation for one branch (solid blue lines in Figs. S1 and S2) and using a constant $\hat{n}$ approximation, $\hat{n} \approx \hat{n}_0$, for the other branch (solid green line in Figs. S1 and S2). The analytical estimates can also be obtained by solving the corresponding expressions (S20) for η_l and (S22) or (S24) for η_u for the parameters $\hat{F}$ or $\hat{v}$.

The parameter $\hat{F}$ contains information about the detachment forces. A large value of $\hat{F}$ indicates that motors can unbind easily while a small value of $\hat{F}$ shows that motors are strongly bound to the filament. Only for small detachment forces or large values of $\hat{F}$ we expect unbinding cascades, which give rise to bistability. Therefore, the critical points of the motility diagram are located in the upper left part of the $(\hat{F}, \frac{N_f}{N})$ parameter plane in Figs. S1. With motor parameters from Table 1 in the main text, the critical points are at $(\hat{F}_c, N_{f,c}/N) = (0.16, 0.84)$, $(5.32, 0.77)$ and $(1.05, 0.80)$ for the three different assays as shown in Figs. S1 A, B and C, respectively. For wild-type and mutant kinesin-1 motors, see Fig. S1 (A), the value $\hat{F} \simeq 2$ is larger than the critical value 0.16; therefore, a transition between a bistable state with bimodal velocity distribution and a state with unimodal velocity distribution is possible as a function of the fraction of fast motors N_f/N. For the other two assays, see Fig. S1 B, C, the value $\hat{F} \simeq 1$ is smaller than the critical values; therefore, the system always stays in a state with unimodal velocity distribution. This agrees with what we obtained from the motility diagrams in the $(\frac{N_f}{N}, \eta)$ parameter plane discussed in the main text.

For the motility diagram in the $(\hat{F}, \frac{N_f}{N})$ plane, the boundaries of the bistable regime are non-monotonous functions of the parameter $\hat{F}$. This gives rise to a re-entrant behavior, which was absent in the $(\frac{N_f}{N}, \eta)$ parameter plane.

The parameter $\hat{v}$ describes the velocity mismatch between slow and fast motors. Small values of $\hat{v}$ correspond to large velocity mismatches. Then, large load forces can build up more easily between slow and fast motors, and we expect unbinding cascades, which give rise to bistability. Therefore, the critical points of the motility diagram are located in the upper right part of the $(\hat{v}, \frac{N_f}{N})$ parameter plane in Figs. S2. With motor parameters from Table 1 in the main text, the critical points are at $(\hat{v_c}$,

$N_{f,c}/N) = (0.47, 0.46)$, $(0.058, 0.87)$, and $(0.096, 0.80)$ for the three different assays as shown in Figs. S2 A, B and C, respectively. The value $\hat{v} \simeq 0.065$ for wild-type and mutant kinesin-1 motors, see Fig. S2 A, is much smaller than the critical value 0.47, whereas the values of $\hat{v}$ are larger than the corresponding critical values for the other two assays. Again, we find that only in the assay with wild-type and mutant kinesin-1 motors a transition from a state with bimodal velocity distribution to a state with unimodal velocity distribution is possible as a function of the fraction of fast motors N_f/N.

4 Influence of the total motor number N

Finally, we discuss the influence of the parameter $N = N_f + N_s$, which is the total number of motors available to attach to the filament, on the average microtubule velocity. The mean-field equation (S17) only depends on $\hat{N} = N_s/N_f$, i.e., if N is changed while $\hat{N}$ is fixed, motility diagrams remain unchanged. This prediction only holds in the mean-field limit of large N.

Using a different approach, Larson *et al.* (9) found that average microtubule velocities as shown in Fig. 3 in the main text depend on N. Within the mean-field approach, average microtubule velocities can only be calculated for unimodal velocity distributions in the regimes of fast and slow transport. For bistable transport, we have to use the master equation approach, see eq. (7) in the main text. Figs. S3 show results for assays with (A) kinesin-II and OSM-3 motors (11) and (B) Xkid and Xklp1 motors (10) and (C) wild-type and mutant kinesin-1 motors (9) for different values of N.

For the assays in Figs. S3 (A) and (B), for which we predict a unimodal velocity distribution, we find that the microtubule velocity is indeed almost independent of N and mean-field and master equation results agree for larger values of N. For the assay in Fig. S3 (C), on the other hand, we predict a transition from a bimodal to a unimodal velocity distribution for $N_f/N \simeq 0.31$. Here we find a sharpening of the transition for increasing N, which can be explained by a sharpening of the bimodal velocity distribution because stochastic switching between the two velocities becomes more unlikely for larger motor numbers N.

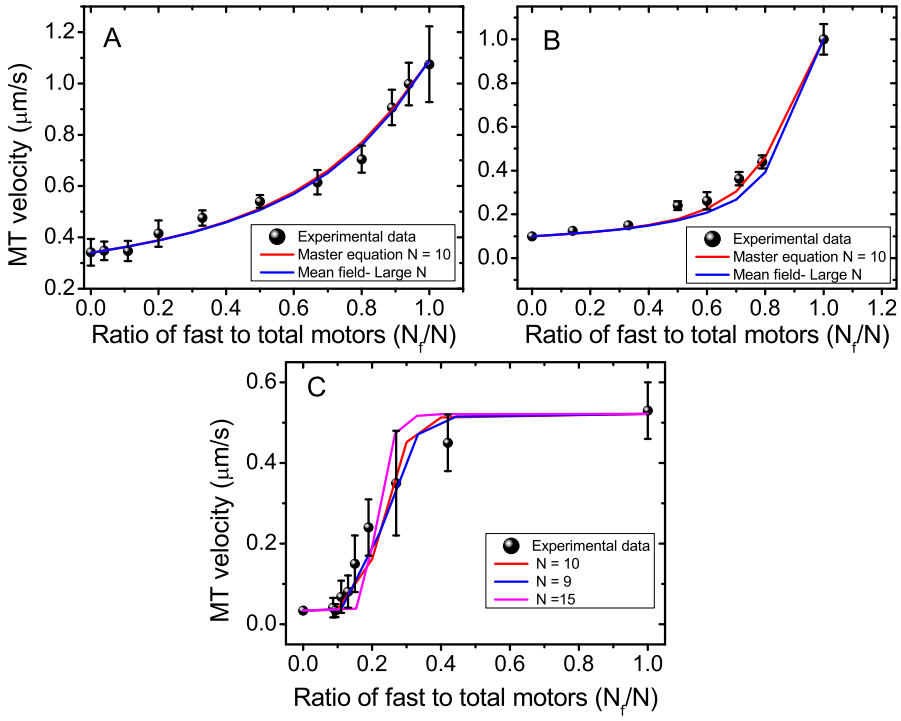

Figure S3: Microtubule velocity as a function of the fraction of fast motors N_f/N for different total numbers of available motors N. Microtubules are transported by (A) OSM-3 and kinesin-II motors (11), (B) Xklp1 and Xkid motors (10), and (C) wild and mutant type of kinesin 1 motors (9). The results for finite $N = 10$ and mean-field results in the limit of large N almost agree for (A) and (B). The transition from bistable to uniform velocities sharpens for increasing N in (C). The data points are the experimental results from Refs. (9–11). The values of motor parameters are given in Table 1 in the main text.

References

1. Klumpp, S., and R. Lipowsky. 2005. Cooperative cargo transport by several molecular motors. *Proc. Natl. Acad. Sci. USA* 102:17284–17289.

2. Müller, M., S. Klumpp, and R. Lipowsky. 2008. Tug-of-war as a cooperative mechanism for bidirectional cargo transport by molecular motors. *Proc. Natl. Acad. Sci. USA* 105:4609–14.

3. Bell, G. 1978. Models for the specific adhesion of cells to cells. *Science* 200:618–627.

4. Svoboda, K., and S. Block. 1994. Force and velocity measured for single kinesin molecules. *Cell* 77:773–784.

5. Kojima, H., E. Muto, H. Higuchi, and T. Yanagida. 1997. Mechanics of single kinesin molecules measured by optical trapping nanometry. *Biophys. J.* 73:2012–22.

6. Visscher, K., M. Schnitzer, and S. Block. 1999. Single kinesin molecules studied with a molecular force clamp. *Nature* 400:184–189.

7. Carter, N., and R. Cross. 2005. Mechanics of the kinesin step. *Nature* 435:308–312.

8. Coppin, C. 1997. The load dependence of kinesin's mechanical cycle. *Proc. Natl. Acad. Sci. USA* 94:8539–8544.

9. Larson, A., E. Landahl, and S. Rice. 2009. Mechanism of cooperative behaviour in systems of slow and fast molecular motors. *Phys. Chem. Chem. Phys.* 11:4890–4898.

10. Bieling, P., I. Kronja, and T. Surrey. 2010. Microtubule Motility on Reconstituted Meiotic Chromatin. *Curr. Biol.* 20:763–769.

11. Pan, X., G. Ou, G. Civelekoglu-Scholey, O. Blacque, N. Endres, L. Tao, A. Mogilner, M. L. a nd R.D. Vale, and J. Scholey. 2006. Mechanism of transport of IFT particles in C. elegans cilia by the concerted action of kinesin-II a nd OSM-3 motors. *J. Cell Biol.* 174:1035–1045.